Composites Science and Technology 137 (2016) 109–117

Contents lists available at ScienceDirect

Composites Science and Technology

journal homepage: http://www.elsevier.com/locate/compscitech

Enhanced conductivity induced by attractive capillary force in ternary conductive adhesive

Hongye Sun*, Xinfeng Zhang, Matthew M.F. Yuen**

Department of Mechanical and Aerospace Engineering, The Hong Kong University of Science and Technology, Clear Water Bay, Kowloon, Hong Kong, China

ARTICLE INFO

Article history:
Received 12 July 2016
Received in revised form
25 October 2016
Accepted 30 October 2016
Available online 1 November 2016

Keywords:
Conductive composite
Electrical conductivity
Thermal conductivity
Capillary force
Pendular bridge

ABSTRACT

Materials with advanced conductive properties are in high demand to fulfill the requirements of energy transport in many fields. Here, we present a simple, efficient yet low cost method to produce highly conductive polymer based composites at low filler concentration of 10 vol%. A particle-wetting fluid as a secondary fluid is introduced to bridge plate-shape silver particles within an epoxy base. The electrical and thermal conductivity dependence on network structure in ternary silver adhesive presenting strong capillary attraction was first reported. Both electrical and thermal conductivities are greatly enhanced by introducing the secondary fluid at a low particle volume fraction of 10%. A non-monotonic dependence of the conductivities on secondary fluid content was observed. The maximum electrical and thermal conductivities correspond to the formation of full pendular network and funicular network, respectively. Gradually increasing the secondary fluid content leads to a microstructure evolution from highly dispersed particles, weak gel network, full pendular network, funicular network and ultimately to compact capillary aggregates network. Such structural transition appears to result from a pendular bridge formation and bridges coalescence. Face-face configuration of plate-shaped silver particles was observed in the pendular state. Taking account of the highly non-spherical shape of silver flake, a bridging gelation model is proposed to explain the underlying mechanism of microstructure transition.

1. Introduction

The development of highly conductive materials has received much attention in electronic packaging due to an increasing demand for high power electronics [1,2]. Conductive particle filled polymer is the most widely used thermal interface material (TIM) because of its low cost, ease of assembly, and re-workability [3,4]. The electrical and thermal performances are significantly influenced by the formation of a particle conductive network, which has been verified by the theoretical model of percolation theory [1,5]. However, in order to achieve a percolative network, a sufficiently high filler loading is required. Commercial silver epoxy as conductive adhesive contains over 20 vol% of silver particles. Table S1 lists state of the art commercial silver epoxy pastes. Thus, reducing filler concentration while maintaining the same level of conductivity is one of the challenging issues for polymer composites.

Referring to the colloidal system, the bulk conductivity enhancement is linked to the formation of a colloidal gel but weakly dependent on filler volume fraction [6,7]. The three dimensional gel networks serve as conducting pathways for electrons and phonons. This inspires the idea to improve the system conductivity by the approach of colloidal gelation at low filler loading.

There is an understanding that gelation could be controlled by tuning the inter-particle attraction even at an extremely low volume fraction [8]. According to the attraction-density (U-Φ) state diagram [9], for low and moderate particle densities, strength of interaction potential plays a dominant role in forming either open clusters or compact aggregation. With gradually increasing the inter-particle attraction, particles grow into transient clusters, a percolative network and a stress-bearing gel network [10]. Meanwhile, morphology of the suspension transits from a fluid-like state to a solid-like state [11].

* Corresponding author.
** Corresponding author.
E-mail addresses: hsun@connect.ust.hk, hsun@ust.hk (H. Sun), meymf@ust.hk (M.M.F. Yuen).

http://dx.doi.org/10.1016/j.compscitech.2016.10.028
0266-3538/

Recently, a capillary force supplied by liquid bridges was reported to create particle network in a colloidal suspension, termed capillary suspension [12]. Depending on the three phase contact angle of secondary fluid on solid within the bulk phase, two types of capillary suspension could be classified. If the contact angle is smaller than 90°, implying that secondary phase wets particle better, pendular bridges form between neighboring particles. Otherwise, if the contact angle is larger than 90°, the particles form clusters around small volumes of the secondary droplets. This is termed as capillary state. The formation of gel network is attributed to the capillary attraction arising from the interfacial free energy reduction in capillary state [13] or negative curvature formation in pendular state [14]. It is believed that capillary interaction is much stronger than the thermal energy governing particle motion [15]. Besides, the strength of capillary attraction shows its controllability in many aspects: by adjusting the secondary fluid content [16], tuning interfacial tension [17], changing colloid size [17] as well as varying mixing process [14]. It is demonstrated to be a convenient yet effective way to tune composite properties without complicated procedures and intricate instruments [18].

Note that Koo et al. [19] reported the effect of capillary attraction on electrical conductivity of silver paste by adding a secondary fluid, flow behavior are adjusted and electrical conductivity is improved by two times. In their report, they adopt spherical silver particles with high loading of 29 vol% and a less preferentially wetted secondary fluid to create the capillary suspension in a capillary state. Secondary fluid needs to be evaporated entirely without collapsing the capillary network. It has been demonstrated that pendular bridges lead to stronger networks than the capillary state [20]. Furthermore plate-shaped particles are reported to yield higher network strength than that of spherical particles [21]. Here, we explore the possibility of building a three-dimensional conductive network by creating capillary suspension in the pendular state with anisotropic silver flakes. We aim to reduce the silver consumption to a lower level of 10 vol% while improving the electrical and thermal conductivities.

The electrical and thermal conductivity dependence on network structure in ternary silver adhesive presenting strong capillary attraction is reported. We examine the structural evolution of ternary blend composition with a secondary wetting liquid loading gradually increased. More specifically, we focus on identifying the microstructure evolution transiting through the maximum electrical and thermal conductivities. In this study, anisotropic silver flakes as fillers and a commercial epoxy as the polymer matrix are employed due to their wide usage as conductive adhesives. A type of ionic liquid (IL) is selected as the secondary fluid which was previously reported [22]. After inducing the aggregation, the IL was cured together with the polymer matrix in the subsequent curing procedure [22]. This in-situ curing of secondary fluid preserves the particle network within the polymer matrix while maintaining the adhesion of the composites.

Morphological observations of capillary induced aggregation were performed using Scanning Electron Microscopy (SEM) and Transmission Electron Microscopy (TEM). We establish a microstructural basis for the electrical and thermal conductivity enhancement. The rheological properties were examined at room temperature using a parallel plate rheometer. Network structure transition was tracked by the composite elasticity, which was extracted within the linear viscoelastic region through dynamic amplitude sweep. The strength of the network featuring a yielding behavior was also characterized by stress ramp. Finally, a bridging gelation model is put forward to show the underlying mechanism of network building by incorporating the effect of anisotropic particle shape.

2. Experimental section

2.1. Materials

High purity silver flakes (99.95%, SF-01C) were obtained from Changcheng Co., Sichuan, China and used as received without any further treatment. The morphology is shown in Fig. S1. The average flake size was 1.12 μm as stated on the datasheet. The thickness of flakes was around 0.05 μm, estimated from the SEM picture (Fig. S1). A widely used liquid epoxy resin based on bisphenol A (D.E.R 331) was supplied by the DOW Chemical Co. An anhydride type hardener (Hexahydro-4-methylphthalic anhydride, mixture of cis and trans, 96%), epoxy curing catalyst (2-Ethyl-4-methylimidazole) and the ionic liquid (1-Butyl-3-methylimidazolium iodide, 99%) as the secondary wetting phase were purchased from Sigma-Aldrich. The mass densities are 1.16 g/ml and 1.49 g/ml for epoxy resin/hardener mixer and IL, respectively.

2.2. Sample preparation

The silver adhesive was prepared using a planetary type mixer (AR-250; Thinky Corp., Tokyo, Japan), which is designed for particle dispersion and air bubble removal. First, the polymer matrix was prepared by mixing the epoxy resin and hardener in a mole ratio of 1:1 based on the epoxide equivalent weight (EEW) of the epoxy resin and the hydroxyl equivalent weight (HEW) of the hardener. Second, silver flakes with a volume fraction of 10% were incorporated in the polymer matrix for 8 min mixing at the simultaneous rotation and revolution speeds of 800 rounds per minute (rpm) and 2000 rounds per minute (rpm). Third, the curing catalyst of 0.5 *wt%* to the polymer mixture was added into the suspension and mixed for 1 min at the same mixing intensity. For the ternary adhesive with secondary fluid, IL was added at the final step. The blends were rotated at 600 rpm, and were revolved at 1500 rpm, simultaneously for 10 s. The mixing intensity was carefully chosen to avoid breaking the particle network. The amount of secondary fluid in the ternary adhesives was quantified by a parameter ρ which is defined as the volume fraction ratio between the secondary liquid and silver flakes, essentially evaluating the coverage of secondary fluid on one single particle. Thus,

$$\rho = \frac{V_{IL}}{V_{Ag}} \tag{1}$$

where V_{IL} is the volume fraction of the secondary fluid and V_{Ag} is the volume fraction of the silver flakes. A series of polymer composites were prepared with varying ρ of 0, 0.018, 0.03, 0.048, 0.067, 0.072, 0.095 and 0.119.

2.3. Three phase wetting angle measurement

The static three phase wetting angle θ of silver-IL-polymer was determined by a modified sessile drop method referred to as the Jung et al. method [23]. The configuration of measurement is shown in Fig. S2. Silver film was deposited on a clean silicon wafer by an e-beam evaporation system (Peva-600EI). The thickness and roughness of the silver film was 195.6 ± 14.5 nm and 3.4 ± 1.5 nm, characterized by a surface profile meter (Tencor P-10 Surface Profiler) and optical 3D profile meter (Bruker NPFLEX 3D Surface Metrology), respectively. The deposited silver film was first placed at the bottom of a glass box filled with the epoxy/hardener mixture. An IL droplet was gently squeezed out from a needle with a diameter of 0.4 mm at the interface between the polymer and the air. The droplet slowly settled down as its shape deformed into an ellipse. An image of the droplet shape was captured after it reached

equilibrium and remained unchangeable, by a digital camera built-in Digidrop contact angle meter. Images obtained were fitted for the three phase wetting angle using SolidWorks, as shown in Fig. S3a. The measurements were conducted five times (Fig. S3b) and the wetting angle was determined to be 45.1 ± 4.0° (listed in Table S2). Since the angle is smaller than 90°, the secondary fluid preferentially wet the particle in the ternary system.

2.4. Fluid-fluid interfacial tension measurement

The measurement of the interfacial tension between the IL and epoxy/hardener mixture was performed using a Spinning Drop Tensiometer (Krüss, SITE 100). The capillary tube was filled with IL as a continuous phase and the polymer droplet was injected into the continuous phase by a long needle. The diameter of the polymer droplet was elongated with centrifugal force correlated with the interfacial tension. The rotation speed varied from 3000 rpm to 9000 rpm. The fitted interfacial tension value started to become constant from 7000 rpm and was determined to be 0.08 mN/m.

2.5. Electrical and thermal conductivity characterization

The four-point electrical conductivity measurement was conducted on a 4156C Precision Semiconductor Parameter Analyzer equipped with a four-probe station. The four in-line probes were evenly separated with a distance of 20 mm. Two adhesive tape strips were placed on a glass slide to control the sample configuration. Silver adhesive was screened onto the glass slide using a doctor blade. A silver adhesive strip was left to be cured at 150 °C for 1 h after removing the tapes. No polishing of the sample surface was made before the conductivity measurement. Electrical resistance of the sample strip was measured using four point probes with sharp probing tips to ensure piercing into the cured sample strip. Each sample strip was tested three times with each measurement taken at different location on the strip. The accurate cross section area was determined by the aforementioned surface profile meter. The electrical conductivity was calculated by Ohm's law. Thermal conductivity measurement was conducted using transient laser flash on an AnterFlashline 3000 thermal diffusivity measurement system. The disk shaped samples, 1 mm thick and 12.7 mm in diameter, were cured at 150 °C for 3 h. The density of the cured samples was determined by the Archimedes' method [24].

2.6. Rheological characterization

Rheological tests were carried out using a 25 mm parallel-plate at a gap of 1 mm on a stress-controlled rheometer (MCR 702 TwinDrive, Anton Paar). The ternary silver adhesives were prepared without a curing catalyst to avoid the curing effect. To create the binary adhesive, silver flakes with a volume fraction of 10% were dispersed in epoxy and hardener mixture using a dissolver stirrer at 800 rpm for 8 min. For the ternary adhesive, the secondary fluid was added to the silver suspension by dissolver mixing at 300 rpm for 40 s followed by a hand premixing. An oscillatory time sweep, of up to 10000 s, was performed for the ternary samples. The results are presented in Fig. S4. No significant change of moduli was observed, eliminating any aging effects during the rheology tests. An oscillatory strain sweeps were examined by imposing an oscillatory strain from 0.01% to 100% at the frequency of 10 rad/s. Dynamic frequency sweeps were performed from 0.01 rad/s to 100 rad/s within the linear viscoelastic region determined in the above dynamic strain sweep. Finally, the stress ramps were carried out to measure the yielding stress (σ_y) which is defined at the point where strain sharply increases [13]. The values were determined by a tangent method [25] and the stress ramps were repeated 3 times for each adhesive. All measurements were made at 20 °C.

2.7. Microstructures observation

The morphology of the particle dispersion and aggregation were observed under a scanning electron microscope (JEOL JSM-6390). Images of particle interconnection within cured ternary adhesive were taken on a transmission electron microscope (JOEL JEM-100CX).

3. Results and discussion

3.1. Effect of secondary fluid contents on conductive performance

Binary and ternary silver epoxy adhesives were cured for electrical and thermal conductivity characterization. The amount of secondary fluid ρ was varied between 0.0 and 0.119. The evolution of conductivities is shown in Fig. 1. It is obvious that the both electrical and thermal conductivities are very sensitive to the addition of IL. The binary adhesive is completely insulating with the conductivity of 10^{-6} S/cm. As ρ increases to 0.03, the electrical conductivity is enhanced to be 10^3 S/cm, transforming the polymer composite from an insulating state to an electrically conductive state. Meanwhile, the thermal conductivity is enhanced by a factor of 6 at $\rho = 0.048$, compared to the binary composite. Noticeably, the conductivity dependence on ρ is not linear but exhibits optimum values. The maximum electrical and thermal conductivity occurred at the content of 0.03 and 0.048, respectively. As ρ exceeds 0.03 and 0.048, further addition of secondary fluid degrades the respective conductivity.

3.2. Effect of secondary fluid contents on microstructure morphology

Conductivities of adhesives are dependent on the particle network structure. To study the non-monotonic dependence of conductivity on the amount of secondary fluid, the corresponding SEM images were taken to review the morphology evolution of the internal microstructure of the ternary composite with different secondary fluid contents, as shown in Fig. 2. A striking morphology transition was observed. For the IL-free sample, silver flakes were randomly distributed in the polymer matrix, shown in Fig. 2a. Adding secondary fluid is believed to give rise to particle

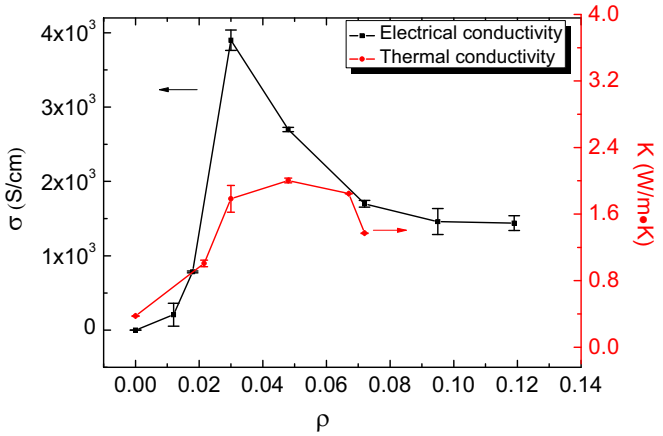

Fig. 1. Electrical and thermal conductivities dependence on the secondary fluid content ρ for silver adhesives with filler volume fraction of 10%. Error bars represent standard deviation from three independent tests.

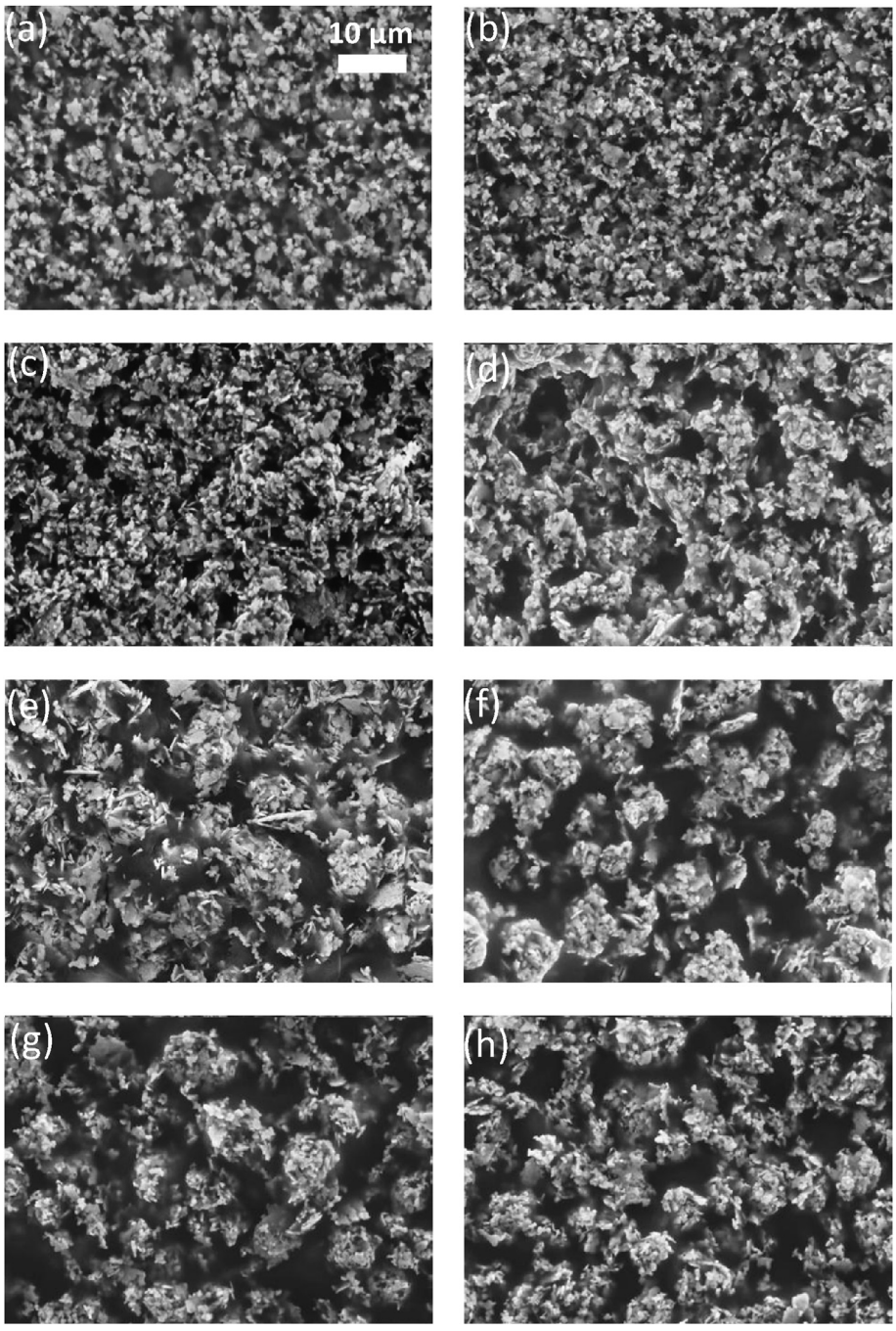

Fig. 2. SEM of Ag-epoxy with different secondary fluid contents ρ added: (a) 0, (b) 0.018, (c) 0.03, (d) 0.048, (e) 0.067, (f) 0.072, (g) 0.096, (h) 0.119. The scale bar shown in (a) is valid for all images.

aggregations. A heterogeneous network is formed providing pathways for electrical and thermal conductivity. Compared with the binary adhesive in Fig. 2a, the morphology change is very limited in the sample with $\rho = 0.018$ (Fig. 2b). However, the sample is already electrically conductive under this circumstance, indicating the existence of a percolative network. As ρ increases to 0.03, the figure shows the likely formation of a well-connected three dimensional network (Fig. 2c). This system-spanning network results from the interconnection of clusters in which silver flakes are possibly connected via the formation of IL pendular bridges. The heterogeneous network accounts for the maximum electrical conductivity as the network formed by the silver flakes forming an optimal set of electrical conduction pathways. When ρ is further increased to 0.048 where maximum thermal conductivity is achieved, more densely packed structures could be observed (Fig. 2d). This likely arises from the supersaturation of the pendular bridges. Neighboring bridges merge together forming funicular structures reported in capillary suspension [16,20] as well as in wet granular materials [26]. Neighboring particles in a funicular state are more intimate than those in a pendular state.

The divergent peak of electrical and thermal conductivities arises from their intrinsic conductive nature. It is well known that electrons can be transmitted across metal particles when the distance between them is less than the electron tunneling distance,

which is normally several nanometers [27]. Electrons can jump from one particle to another without direct contact. Heat conduction depends primarily on phonon transport with electon transport being a minor component. Phonon transport requires more intimate physical contact of particles [28]. As the conductive pathways are formed by capillary bridges, electrical conductivity is first attained with the possible formation of a heterogeneous bridge network with silver flakes in the branches having gaps less than the electron tunneling distance threshold. With increase of IL to $\rho = 0.048$, more compact funicular bridges are formed with direct contact between silver flakes leading to improved thermal conductivity. The anisotropic geometry of the silver flakes also helps enhance the contact area with particles facilitating the conductivity. Compacting of the bridges would reduce the number of connecting pathways and this reduces the electrical conductivity. Thus, funicular structure is beneficial to the thermal conductivity but detrimental to the electrical conductivity.

Further addition of secondary fluid beyond $\rho = 0.048$ results in decrease of both electrical and thermal conductivity because of the formation of compact aggregates, as observed in Fig. 2e–h with ρ varying from 0.067 to 0.119. This is consistent with the results observed in the capillary aggregates network formation among spherical particles [16]. The aggregates formation likely arises from the expansion of the secondary droplet size [16], which is supported by confocal microscope images reported by Koos et al. [20] as well as optical microscope images in wet granular materials [29]. The ionic liquid we used contains a very unique iodide, which allows us to element mapping to track the position of secondary fluid. SEM-EDS analysis in Fig. S5 shows that the distribution of iodine element covers the silver aggregation, indicating that silver particles are immersed in the IL droplet.

To further confirm structural transition and characterize the gel network formation, flowing and rheological properties are examined.

3.3. Effect of secondary fluid contents on rheology

Adding secondary fluid dramatically changes the flow of suspensions due to the presence of particle clustering and network [12,30]. Like most capillary driven systems, a striking liquid to solid transition was observed in our system, as shown in Fig. 3. Binary adhesive is a typical semi-dilute suspension. Comparatively, the sample with $\rho = 0.018$ shows an increased viscosity, but could still spread on the substrate. The absence of free flow starts at $\rho = 0.03$, exhibiting a paste-like morphology. At $\rho = 0.048$, the ternary adhesive turns to be semi-solid with apparent slurry morphology. With further increasing ρ, this morphology change becomes more striking. This apparent phase transition is compelling evidence of gelation, which is further evaluated by rheological measurements.

Oscillatory amplitude and frequency sweeps and stress ramps are conducted to probe the elasticity and strength of the particle network, respectively. Oscillatory amplitude sweeps characterize the visco-elastic behavior of samples by detecting the strain dependent moduli response. The solid particle concentration was fixed at $\varphi = 10\%$ and ρ varies from 0 to 0.072, which are consistent with the samples for conductivity measurement. The plateau storage modulus (G'_p) was determined from the linear viscoelastic region (LVER) where G' and G'' are strain independent [31,32]. Storage moduli under strain of 0.01% and frequency of 10 rad/s were taken as G'_p. To further confirm the value of G'_p, oscillatory frequency sweeps within LVER were conducted and G'_p was determined under same condition (strain of 0.01% and frequency of 10 rad/s). Oscillatory amplitude sweeps are shown in Fig. S6a ($\rho = 0$–0.03) and S6b ($\rho = 0.039$–0.072).

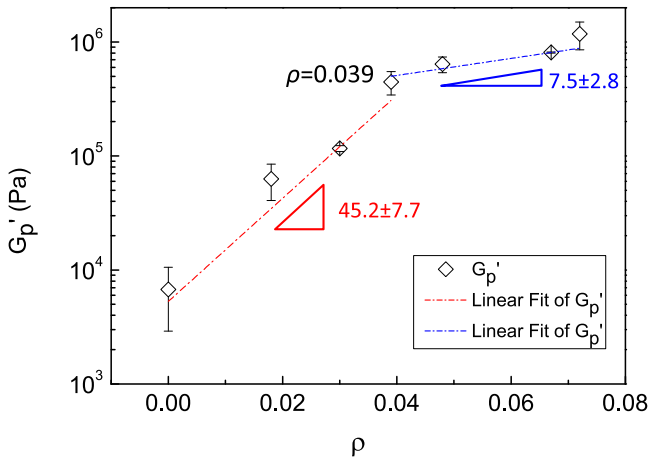

Fig. 4. Plateau storage modulus G'_p in a logarithmic scale extracted from LEVR of amplitude and frequency sweeps. Error bars represent standard deviation of G'_p extracted from amplitude and frequency sweeps. G'_p was linearly fitted by a red dashed line and a blue dashed line. Red and blue triangles represent the slops of the apparent fittings in two regimes, respectively. Turning point occurs at $\rho = 0.039$ shown in the figure. (For interpretation of the references to colour in this figure legend, the reader is referred to the web version of this article.)

The dependence of G'_p in a logarithmic scale on ρ is depicted in Fig. 4. Two different regimes can be distinguished by the two differing slopes of G'_p, which corresponds to two different types of network structures (open cluster and compact cluster) [10,33]. The two slopes are obtained from linear fittings. For ρ varying from 0 to 0.039 (regime *I*), G'_p shows a pronounced increase with a growth slope of 45.2 ± 7.7, indicating the rapid growth of open clusters. With ρ beyond 0.039, the growth of G'_p is less sensitive to ρ with a much flat slope of 7.5 ± 2.8 (Regime *II*). This is due to the formation of more compact aggregates.

For clusters in regime *I*, the elasticity is dominated by the deformation of particle-particle linkage and the elastic constant depends on the cluster backbone size. As ρ increases, the arrested probability *P* of free silver flakes is increased due to the increased bridge number and size. As a result, the cluster density and correlation length grow rapidly. Upon clusters interconnecting to form a space-spanning network, the gelation boundary is approached and G'_p increases qualitatively. At $\rho = 0.018$, a weak gel network forms, indicated by the oscillatory frequency sweeps where G′ and G'' are

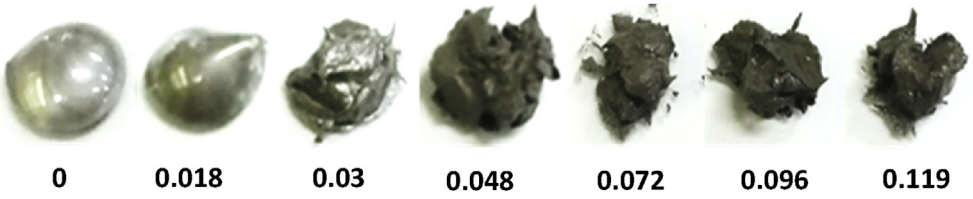

Fig. 3. Macroscopic observation of the transition from fluid-like behavior to solid-like behavior with different ρ.

both frequency independent, as shown in Fig. S7a. The weak gel network formation is consistent with silver flake composite the conductive state featuring low conductivity. The weak network as well as the low conductivity comes from the insufficient bridging bonds. The bond inside the network is likely a mixture of pendular bridges and overlaps of flakes. At the turning point of $\rho = 0.039$, the cessation of rapid growth indicates the saturation of bridge number and size. Most particles are bonded by pendular bridges and bridge strength reaches the maximum, indicating the formation of the full pendular network [16]. This full pendular network accounts for the maximum electrical conductivity and agrees with the heterogeneous structure of the SEM image in Fig. 2c.

In regime *II*, flakes aggregate into compact clusters, as shown in Fig. 2. The compact clusters form bonds with other compact clusters. The overall elasticity of the network is dominated by the inter-cluster linkage [34]. For compact clusters, the elastic modulus can be scaled as $G' \sim k/\xi$ [10]. Here, k is the inter-particle elastic constant and ξ is the compact cluster correlation length. As ξ decreases due to aggregates formation, G' increases accordingly. For high ρ, cluster size is approaching saturation and only shrinks slightly and thus the growth of G'_p slows down. Electrical conductivity drops slowly and tends to plateau as shown in Fig. 1.

The network strength is characterized by yield stress σ_y, beyond which shearing stress will lead to the breakdown of the particle network. Ternary adhesive features a high yield stress due to the gel network formation. Typical deformations versus stress curves for a broad range of ρ are shown in Fig. S8. Determination of yield stress is illustrated in supplement. The ρ dependence of σ_y is plotted in Fig. 5. σ_y shows a non-monotonic evolution with a clear distinction of rise, peak and drop. As ρ increases from 0 to 0.039, σ_y grows slowly with a plateau between 0.03 and 0.039. This plateau is speculated to be the transition from the pendular network to funicular structure and full pendular network occurs at $\rho = 0.03$. A prominent increase occurs in the range of 0.039–0.048, and later σ_y drops to another plateau value. The rise and drop arise from the network formation and compact aggregates, as established in the previous section.

It is worth noting that peak yield stress occurs at $\rho = 0.048$, would correspond to the funicular network structure, which agrees with others' observations that yield stress drops when compact aggregation forms [16,21]. The reasons for maximum yields stress occurring at funicular structure is not yet clear. It is speculated that the concave liquid-liquid interface induces a negative Laplace pressure which pulls particles into a more intimate contact. The inter-particle friction forces increase accordingly, which is likely to be responsible for the maximum yield stress. The increased intimacy among particles also explains the maximum thermal conductivity at the funicular structure. As that electron transport of a network depends on quantum tunneling effect which does not require direct contact of the particles forming conducting pathways [35,36], whereas the network strength depends on direct contact of interparticle connection within the cluster [37,38]. Because clusters become more compact at funicular state and possibly reduce the number of conducting pathways, electrical conductivity drops while yield stress reaches the maximum.

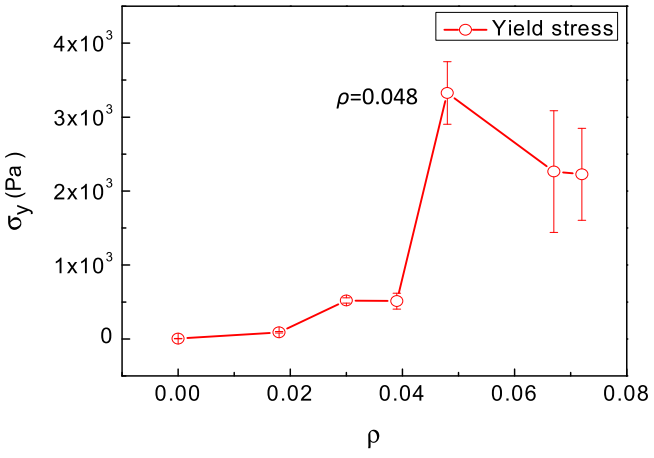

Fig. 5. Yield stress as a function of ρ obtained from stress ramps. Error bars represent standard deviation from three independent tests. Maximum yield stress exists at $\rho = 0.048$ shown in the figure.

G'_p and σ_y exhibit opposite trends with ρ beyond 0.048. The plateau storage modulus evaluates the overall ability of the particle network to resist the deformation. Yield stress characterizes the onset of network breakup, in other words, the strength of the weakest network. σ_y not only depends on the network elasticity but also the yield strain.

3.4. Proposed bridging mechanism

3.4.1. Bridging configuration and saturation size

TEM images were taken to reveal particle interconnection in the pendular state and capillary aggregates. 3D schematic drawings of particle arrangements are inserted in TEM images. Paired silver flakes are bridged in a face-face configuration at the pendular state and form chain-like cluster, as shown in Fig. 6a. Notably, the coordination number Z, i.e. the number of bridges that each particle possesses, is estimated to be 2 from the TEM image. Regarding the capillary aggregation, particles connection becomes more compact and cluster contains multi-particles aggregation instead of the pendular chain-like cluster, as shown in Fig. 6b. This is consistent with the SEM observation in Fig. 2e. This may because size of IL droplet is larger than that of silver flakes and silver flakes are predominantly distributed within the IL droplet. This shows strong affinity with a plate-shape particle stabilized emulsion [39]. The element mapping in Fig. S5 also shows that the distribution of silver flakes overlaps with that of IL, implying that silver flake connecting with the IL droplet.

For TIM applications, high electrical and thermal conductivity and yet low viscosity are desired. Considering these requirements, compact aggregates need to be strictly avoided, which makes the determination of saturation concentration extremely important. To proceed further, we estimate the saturation size of a pendular bridge, which is the most likely full pendular network structure for the optimal electrical conductivity in the silver epoxy. As discussed in the earlier sections, the funicular network is evolved out of the pendular network with further particle aggregation.

Experimentally, a full pendular network with $\rho = 0.03$ is assumed to be the condition before which bridge coalescence occurs. In the two dimension (2D) TEM images shown in Fig. 6a, the coordination number $Z = 2$ is the meniscus number per particle. In three dimensional (3D) system, in order to form a particle network, Z must be larger than 2. A recent study on anisotropic colloids [40] subjected to strong attraction shows that, anisotropic discoids favor Face-Face configuration featuring a low mean contact number of 3.2 ± 0.9 in a 3D system. Thus, it is suggested that $Z = 3$ would be appropriate in consideration of the anisotropic geometry of the silver flake.

According to the definition of ρ,

$$\rho = \frac{V_{IL}}{V_{Ag}} = \frac{N_{pb}V_{pb}}{N_{Ag}V_{Ag}} = \frac{Z/2N_{Ag}V_{pb}}{N_{Ag}V_{Ag}} = \frac{ZV_{pb}}{2V_{Ag}} \quad (2)$$

where N_{pb} and N_{Ag} are the total number of pendular bridges and

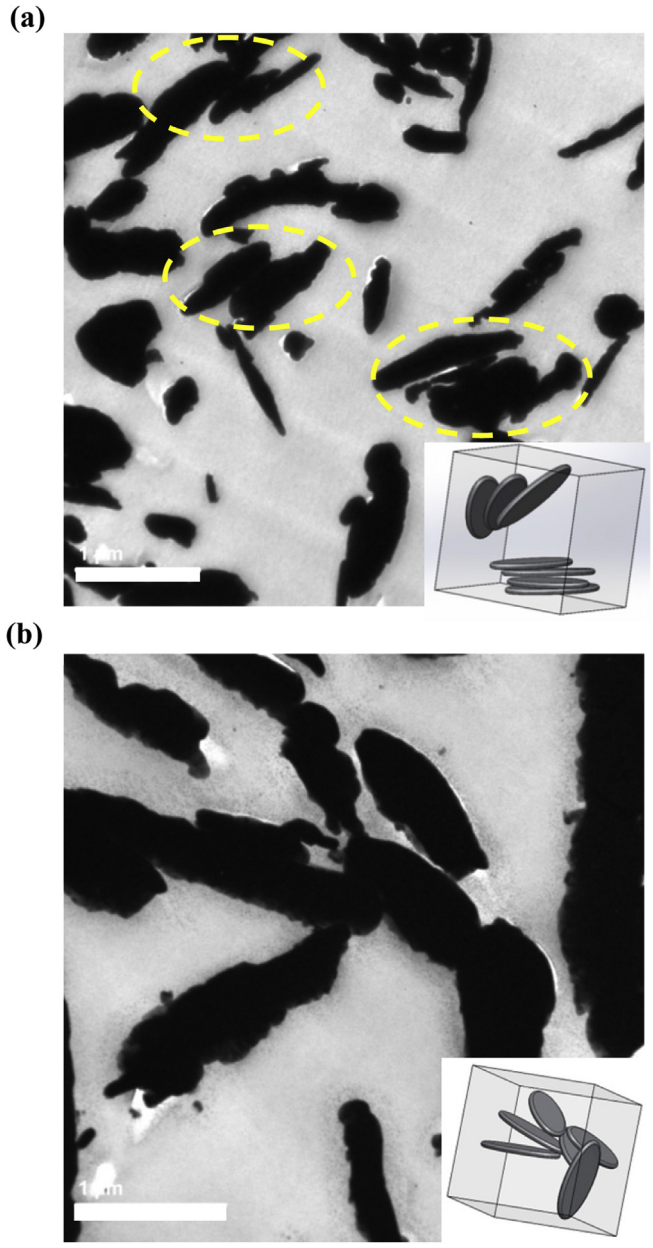

Fig. 6. TEM images of silver flakes connection in ternary adhesive with a silver volume fraction of 10%. Insert shows a 3D schematic drawing of particle arrangements accordingly. (a) $\rho = 0.03$, particles in a pendular state prefer a face-face configuration and form chain-like cluster, as highlighted by the yellow dashed ellipse; (b) $\rho = 0.119$, particles connection becomes more compact and cluster is more condense. (For interpretation of the references to colour in this figure legend, the reader is referred to the web version of this article.)

silver flakes, respectively; V_{pb} and V_{Ag} are the volumes of single pendular bridge and single silver flake, respectively.

Silver flakes are taken as thin elliptic cylinders and assumed to be identical in size. Estimated from SEM image (Fig. S1), $a = 1$ μm is the semi-major axis, $b = 0.5$ μm is the semi-minor axis and flake thickness $t = 0.12$ μm is the height of the cylinder. Thus, the volume of a single silver flake is expected to be $V_{Ag} = \pi abt = 0.188$ μm^3. Then, the bridge volume V_{pb} is estimated to be 5.64×10^{-3} μm^3. Furthermore, treating the meniscus as having cylindrical edges, the geometric criterion of bridge coalescence is where the surface of a silver flake is fully covered by secondary fluid. Calculated from the bridge volume and silver surface area, the height of the bridge is determined to be 2.4 nm, which is also the distance between neighboring flakes. The bridge height is much smaller than the silver surface dimension, which makes the assumption of cylindrical edges of the bridge practicable. As mentioned above, the electron tunneling distance is smaller than 10 nm. Thus, inter-particle distance of 2.4 nm is reasonable for electron transport between neighboring silver flakes.

3.4.2. *Bridging gelation induced by secondary wetting liquid*

Combining the conductivity, microstructure and rheology results, it is reasonable to suggest that the maximum electrical and thermal conductivities occur at the formation of a full pendular network and funicular network within the gelation region. A structural evolution from highly dispersed particles, weak gel network, full pendular network and ultimately to compact capillary aggregates network was observed. Such a transition is analogous to the behavior of many colloidal systems where gelation of particles is driven by inter-particle attraction potential U, including non-absorbing polymer induced depletion [40] and absorbing polymer induced bridging attraction [41]. In these systems, the attraction strength is tuned by the concentration of the polymer. Within this framework, the addition of secondary fluid will produce an effective attraction potential between particles. The attractive strength is sensitive to the volume fraction ratio ρ between secondary fluid and solid flakes, which simply characterize the surface coverage of secondary fluid on particles. The value of ρ determines the type of gel network structure, either pendular network or capillary aggregates network. Based on the current results, a physical model of bridging gelation is proposed to illustrate the underlying network transition, shown in Fig. 7.

Without the IL, silver flakes were distributed randomly and stably in the polymer base (Fig. 7a), and particle interaction is dominated by the van der Waals force. When IL is added, silver flake is preferably wetted by IL. The IL droplets are adhered to the silver flake surface. When a IL wetted silver flake approaches another wetted silver flake within sufficient proximity, the cohesive force of the IL would cause the formation of a pendular bridge with a face-face configuration. The probability of a bridge formation partially depends on the droplet size and droplet number. Thus, bridging attraction leads silver flakes to connect into clusters. In Fig. 7b, when more IL is added, clusters grow into a conductive network with a combination of IL bridged particles and particle-particle binding by van der Waals forces. In this case, the conductive network is very weak and silver flake composite exhibits low conductivities. Until most of the silver flakes are bridged by IL droplets and the space filling network is formed largely via bridging connections, that is, approaching bridge saturation, the full pendular network forms. This network structure is schematically shown in Fig. 7c. Elasticity depends on the inter-particle bridging and electrical conductivity reaches the maximum. After the bridge becomes saturated, excessive addition of IL will merge neighboring bridges into a larger cluster resulting in a funicular structure. Silver flakes are pulled into more intimate contact, as shown in Fig. 7d. The funicular structure presents the maximum yield stress and peak thermal conductivity. Elasticity falls into the second regime, where inter-cluster link dominates the elastic response.

As the droplet size of the secondary fluid grows larger than the size of silver flakes, silver particles favor to distribute in the secondary fluid which drives silver flakes to form capillary aggregates, shown in Fig. 7e. As a consequence, the connections between aggregates weaken. The platelet geometry of silver flakes affects packing configuration inside the cluster.

Not surprisingly, bridging gelation is not only realized by the liquid phase. A similar phenomenon was reported in micro-gel bridged colloids [42–44]. Despite the differences of the bridge

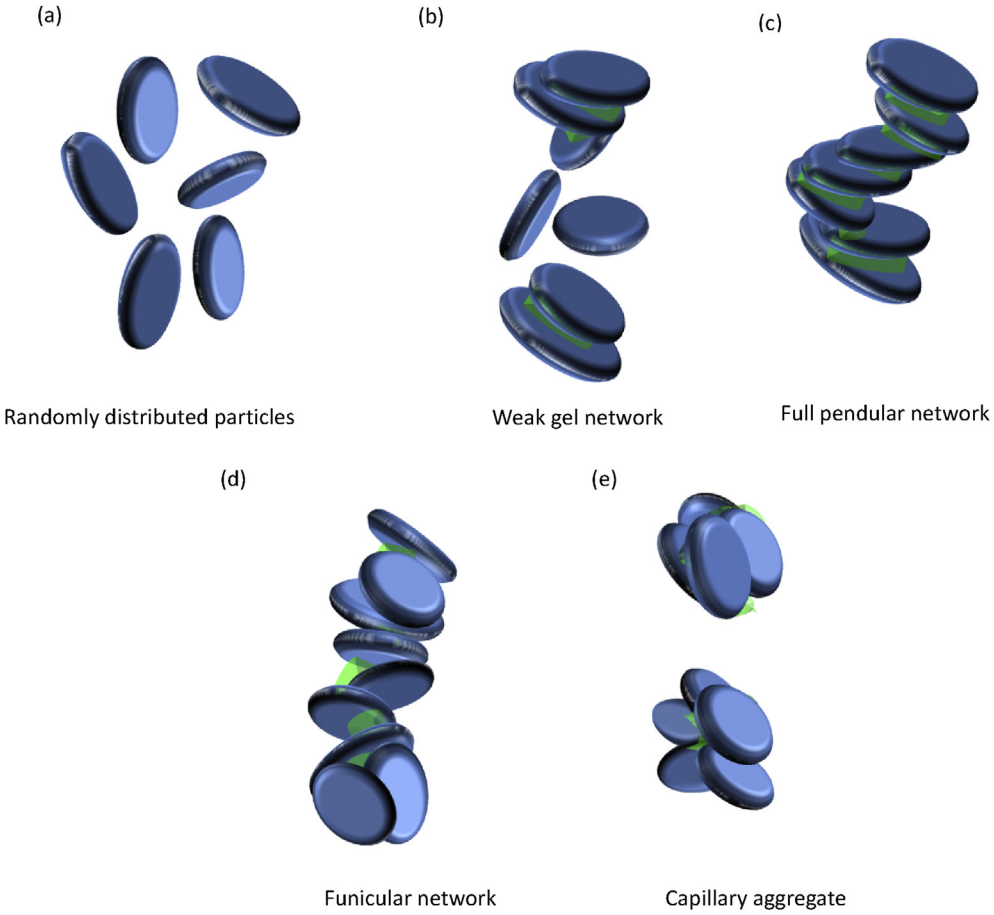

Fig. 7. Schematics of how secondary fluid content ρ affects the microstructure. Green area represents secondary fluid and particles are shown as blue ellipses. (a) Silver flake suspension in the epoxy adhesive with IL-free. (b) Weak gel network resulting from pendular bridge formation and particle overlap. (c) Full pendular network where bridges are saturated. (d) Funicular network from oversaturated bridge coalescence. (e) Compact capillary aggregates. (For interpretation of the references to colour in this figure legend, the reader is referred to the web version of this article.)

formation (liquid & gel), they both share common dependence on the wetting properties of ternary systems. Polymer gel was adsorbed on the solid particle because of the hydrophobic interaction [42] while secondary liquid in our silver flake composites was attached to the silver surface because of favorable wetting property. Interfacial energy reduction drives bridge formation and secondary liquid concentration tunes the attraction strength. The microstructure transition highly depends on surface coverage and bridge saturation.

4. Conclusion

This article reports the electrical and thermal performance of secondary fluid bridged ternary composites. A non-monotonic dependence of conductivities on secondary fluid content is observed. Morphological and rheological properties of ternary silver adhesives were studied to look into the microstructure. It is found that, with increasing the concentration of the secondary liquid IL, microstructure transits from a dispersed state, a weak gel network, full pendular network, funicular network and finally to compact aggregation. The microstructure transition highly depends on surface coverage and bridge saturation. The maximum electrical and thermal conductivities correspond to the turning point of elasticity and maximum yield stress, which are full pendular network and funicular network, respectively. Face-face configuration of platelet-shape particles bridging were imaged by TEM. A bridging gelation model is put forward to illustrate the structural transition.

Notes

The authors declare no competing financial interest.

Acknowledgments

This work was financially supported by the Research Grants Council of Hong Kong [grant number 622013]. The authors would like to acknowledge the assistance from Dr. Stephen Kwok, Dr. Yinsheng Zhong, Dr. Kandy Yeung and Mr. Zhibo Chen.

Appendix A. Supplementary data

Supplementary data related to this article can be found at http://dx.doi.org/10.1016/j.compscitech.2016.10.028.

References

[1] Y.-H. Ji, Y. Liu, G.-W. Huang, X.-J. Shen, H.-M. Xiao, S.-Y. Fu, Ternary Ag/epoxy adhesive with excellent overall performance, ACS Appl. Mater. Interfaces 7 (2015) 8041–8052.
[2] H. Shen, J. Guo, H. Wang, N. Zhao, J. Xu, Bioinspired modification of h-BN for high thermal conductive composite films with aligned structure, ACS Appl. Mater. Interfaces 7 (2015) 5701–5708.
[3] R. Linderman, T. Brunschwiler, B. Smith, B. Michel, High-performance thermal

interface technology overview, in: Thermal Investigation of ICs and Systems, 2007. THERMINIC 2007. 13th International Workshop, IEEE, 2007, pp. 129–134.
[4] M. Knaapila, O.T. Rømoen, E. Svåsand, J.P. Pinheiro, Ø.G. Martinsen, M. Buchanan, A.T. Skjeltorp, G. Helgesen, Conductivity enhancement in carbon nanocone adhesive by electric field induced formation of aligned assemblies, ACS Appl. Mater. Interfaces 3 (2011) 378–384.
[5] A. Devpura, P.E. Phelan, R.S. Prasher, Percolation theory applied to the analysis of thermal interface materials in flip-chip technology, in: Thermal and Thermomechanical Phenomena in Electronic Systems, 2000. ITHERM 2000. The Seventh Intersociety Conference on, vol. 1, IEEE, 2000.
[6] B. Nigro, C. Grimaldi, P. Ryser, F. Varrato, G. Foffi, P.J. Lu, Enhanced tunneling conductivity induced by gelation of attractive colloids, Phys. Rev. E 87 (2013) 062312.
[7] A.V. Kyrylyuk, M.C. Hermant, T. Schilling, B. Klumperman, C.E. Koning, P. Van der Schoot, Controlling electrical percolation in multicomponent carbon nanotube dispersions, Nat. Nanotechnol. 6 (2011) 364–369.
[8] S. Manley, L. Cipelletti, V. Trappe, A. Bailey, R.J. Christianson, U. Gasser, V. Prasad, P. Segre, M. Doherty, S. Sankaran, Limits to gelation in colloidal aggregation, Phys. Rev. Lett. 93 (2004) 108302.
[9] E. Zaccarelli, Colloidal gels: equilibrium and non-equilibrium routes, J. Phys. Condens. Matter 19 (2007) 323101.
[10] M. Laurati, G. Petekidis, N. Koumakis, F. Cardinaux, A.B. Schofield, J.M. Brader, M. Fuchs, S.U. Egelhaaf, Structure, dynamics, and rheology of colloid-polymer mixtures: from liquids to gels, J. Chem. Phys. 130 (2009) 134907.
[11] V.J. Anderson, H.N. Lekkerkerker, Insights into phase transition kinetics from colloid science, Nature 416 (2002) 811–815.
[12] E. Koos, N. Willenbacher, Capillary forces in suspension rheology, Science 331 (2011) 897–900.
[13] E. Koos, N. Willenbacher, Particle configurations and gelation in capillary suspensions, Soft Matter 8 (2012) 3988–3994.
[14] T. Domenech, S. Velankar, Capillary-driven percolating networks in ternary blends of immiscible polymers and silica particles, Rheol. Acta 53 (2014) 593–605.
[15] N. Mitarai, F. Nori, Wet granular materials, Adv. Phys. 55 (2006) 1–45.
[16] T. Domenech, S.S. Velankar, On the rheology of pendular gels and morphological developments in paste-like ternary systems based on capillary attraction, Soft Matter 11 (2015) 1500–1516.
[17] E. Koos, J. Johannsmeier, L. Schwebler, N. Willenbacher, Tuning suspension rheology using capillary forces, Soft Matter 8 (2012) 6620–6628.
[18] M. Xu, H. Liu, H. Zhao, W. Li, How to decrease the viscosity of suspension with the second fluid and nanoparticles? Sci. Rep. 3 (2013).
[19] M. Schneider, E. Koos, N. Willenbacher, Highly conductive, printable pastes from capillary suspensions, Sci. Rep. 6 (2016) 31367.
[20] F. Bossler, E. Koos, Structure of particle networks in capillary suspensions with wetting and nonwetting fluids, Langmuir 32 (2016) 1489–1501.
[21] J. Maurath, B. Bitsch, Y. Schwegler, N. Willenbacher, Influence of particle shape on the rheological behavior of three-phase non-brownian suspensions, Colloids Surf. A Physicochem. Eng. Asp. 497 (2016) 316–326.
[22] X. Zhang, M.M.-F. Yuen, High performance electrical conductive composites with ultralow percolation threshold, in: Electronic Packaging Technology (ICEPT), 2014 15th International Conference on: IEEE, 2014, pp. 306–309.
[23] Y.C. Jung, B. Bhushan, Wetting behavior of water and oil droplets in three-phase interfaces for hydrophobicity/philicity and oleophobicity/philicity†, Langmuir 25 (2009) 14165–14173.
[24] Z. Zhang, Processing and Characterization of Micro-scale and Nanscale Silver Paste for Power Semiconductor Device Attachment, Virginia Polytechnic Institute and State University, 2005.
[25] U. Teipel, Energetic Materials: Particle Processing and Characterization, John Wiley & Sons, 2006.
[26] S. Strauch, S. Herminghaus, Wet granular matter: a truly complex fluid, Soft Matter 8 (2012) 8271–8280.
[27] E. Sancaktar, L. Bai, Electrically conductive epoxy adhesives, Polymers 3 (2011) 427–466.
[28] P. Keblinski, S. Phillpot, S. Choi, J. Eastman, Mechanisms of heat flow in suspensions of nano-sized particles (nanofluids), Int. J. Heat Mass Transf. 45 (2002) 855–863.
[29] M. Scheel, R. Seemann, M. Brinkmann, M. Di Michiel, A. Sheppard, B. Breidenbach, S. Herminghaus, Morphological clues to wet granular pile stability, Nat. Mater. 7 (2008) 189–193.
[30] S. Hoffmann, E. Koos, N. Willenbacher, Using capillary bridges to tune stability and flow behavior of food suspensions, Food Hydrocoll. 40 (2014) 44–52.
[31] J.C. Berg, An Introduction to Interfaces & Colloids: the Bridge to Nanoscience, World Scientific, 2010.
[32] R.K. Pujala, Dispersion Stability, Microstructure and Phase Transition of Anisotropic Nanodiscs, Springer, 2014.
[33] S. Shah, Y.-L. Chen, K. Schweizer, C. Zukoski, Viscoelasticity and rheology of depletion flocculated gels and fluids, J. Chem. Phys. 119 (2003) 8747–8760.
[34] A. Zaccone, H. Wu, E. Del Gado, Elasticity of arrested short-ranged attractive colloids: homogeneous and heterogeneous glasses, Phys. Rev. Lett. 103 (2009) 208301.
[35] C.-W. Nan, Y. Shen, J. Ma, Physical properties of composites near percolation, Annu. Rev. Mater. Res. 40 (2010) 131–151.
[36] D. Toker, D. Azulay, N. Shimoni, I. Balberg, O. Millo, Tunneling and percolation in metal-insulator composite materials, Phys. Rev. B 68 (2003) 041403.
[37] S. Feng, P.N. Sen, Percolation on elastic networks: new exponent and threshold, Phys. Rev. Lett. 52 (1984) 216.
[38] J. Mewis, N.J. Wagner, Colloidal Suspension Rheology, Cambridge University Press, 2012.
[39] Y. Nonomura, N. Kobayashi, Phase inversion of the Pickering emulsions stabilized by plate-shaped clay particles, J. Colloid Interface Sci. 330 (2009) 463–466.
[40] L.C. Hsiao, B.A. Schultz, J. Glaser, M. Engel, M.E. Szakasits, S.C. Glotzer, M.J. Solomon, Metastable orientational order of colloidal discoids, Nat. Commun. 6 (2015).
[41] K. Pickrahn, B. Rajaram, A. Mohraz, Relationship between microstructure, dynamics, and rheology in polymer-bridging colloidal gels, Langmuir 26 (2009) 2392–2400.
[42] C. Zhao, G. Yuan, D. Jia, C.C. Han, Macrogel induced by microgel: bridging and depletion mechanisms, Soft Matter 8 (2012) 7036–7043.
[43] C. Zhao, G. Yuan, C.C. Han, Bridging and caging in mixed suspensions of microsphere and adsorptive microgel, Soft matter 10 (2014) 8905–8912.
[44] J. Luo, G. Yuan, C. Zhao, C.C. Han, J. Chen, Y. Liu, Gelation of large hard particles with short-range attraction induced by bridging of small soft microgels, Soft matter 11 (2015) 2494–2503.